Geochemistry Geophysics Geosystems G3
AN ELECTRONIC JOURNAL OF THE EARTH SCIENCES
Published by AGU and the Geochemical Society

Article
Volume 4, Number 1
3 January 2003
1002, doi:10.1029/2002GC000326
ISSN: 1525-2027

Degassing and contamination of noble gases in Mid-Atlantic Ridge basalts

P. Burnard
Department of Earth Sciences, University of Manchester, Manchester M13 9PL, United Kingdom

Now at Department of Earth and Space Sciences, University of California, Los Angeles, Los Angeles, California 90095, USA. (peteb@argon.ess.ucla.edu)

D. Harrison
Department of Earth Sciences, University of Manchester, Manchester M13 9PL, United Kingdom

Now at Institute Isotopengeologie/Mineral. Rohstoffe, NO F 64, ETH Zentrum CH-8092, Zürich, Switzerland. (harrison@erdw.ethz.ch)

G. Turner
Department of Earth Sciences, University of Manchester, Manchester M13 9PL, United Kingdom (grenville.turner@man.ac.uk)

R. Nesbitt
Southampton Oceanography Centre, University of Southampton, Waterfront Campus, European Way Southampton SO17 1BJ, United Kingdom (rwn1@southampton.ac.uk)

[1] New He, Ne, Ar and CO_2 stepped-crushing data from the Mid-Atlantic Ridge show that contamination of basalts by atmospheric noble gases involves three or more components: unfractionated air, fractionated air with high $^{36}Ar/^{22}Ne$ ($\geq$45) and fractionated air with low $^{36}Ar/^{22}Ne$ ($\leq$5). In addition, the magmatic noble gases trapped in these basaltic glasses are variably fractionated such that $^{4}He/^{40}Ar^*$ (where the asterisk indicates corrected for atmospheric contamination based on all ^{36}Ar being atmospheric in origin) is in the range 3–12. Single samples have a range in $^{4}He/^{40}Ar^*$ with the highest ratios in the final crush steps, consistent with the most fractionated (highest $^{4}He/^{40}Ar^*$) volatiles trapped in the smallest vesicles. It is not possible to distinguish between batch and Rayleigh degassing mechanisms. The complexities of the contamination and magmatic fractionation processes means that it is not possible to estimate $^{40}Ar/^{36}Ar$ of the mantle source to these basalts other than it must be higher than the highest ratio measured (26,200 ± 5200). Noble gas/CO_2 ratios are also variable. While some CO_2 adsorption during crushing exaggerates the variations in He/CO_2 and Ar/CO_2, we show that it is not possible to account for the entire variation as an analytical artefact: some of the variation is present in the vesicles. Variations in He/CO_2 cannot be attributed to solubility controlled degassing because of the broadly similar solubilities of He and CO_2 in tholeiitic magmas. The large range in He/CO_2 in these glasses (factor of 10) is not accompanied by indications of major changes in melting regime or source region chemistry, therefore is thought to reflect late-stage (magmatic) fractionation of CO_2 from the noble gases. It is not possible to identify an explicit mechanism, although both CO_2 reduction (e.g., to hydrocarbons or graphite) and kinetic CO_2-noble gas fractionation could account for the variations.

Components: 10,131 words, 7 figures, 3 tables.

Keywords: basalt; mid-ocean ridge; carbon dioxide; helium; argon; degassing.

Index Terms: 1025 Geochemistry: Composition of the mantle; 1040 Geochemistry: Isotopic composition/chemistry; 3035 Marine Geology and Geophysics: Midocean ridge processes; 3670 Mineralogy and Petrology: Minor and trace element composition.

Received 6 February 2002; **Revised** 20 June 2002; **Accepted** 2 July 2002; **Published** 3 January 2003.

Burnard, P., D. Harrison, G. Turner, and R. Nesbitt, Degassing and contamination of noble gases in Mid-Atlantic Ridge basalts, *Geochem. Geophys. Geosyst.*, *4*(1), 1002, doi:10.1029/2002GC000326, 2003.

1. Introduction and Previous Work

[2] Studies of noble gases in oceanic basalts have the potential to trace the development of chemical heterogeneities in the mantle. While the He and Ne isotopic structure of the mantle have been broadly established [see for example, the review by *Farley and Neroda*, 1998], and the mantle Ar isotopic structure is becoming progressively more clear [*Trieloff et al.*, 2002; *Harrison et al.*, 1999; *Moreira et al.*, 1998; *Trieloff et al.*, 2000; *Valbracht et al.*, 1997], the relative abundances of the noble gases – especially relative abundances of primordial noble gas isotopes – in the mantle are poorly constrained. This contribution is part of an ongoing effort using combined noble gas and CO_2 determinations to characterize relative noble gas abundances in the mantle. Using noble gas – CO_2 analyses of glasses from the Mid-Atlantic Ridge, we demonstrate how mantle compositions can be distinguished from atmospheric contamination and elemental fractionation during transport.

1.1. Noble Gas Fractionation During Magmatic Processes

[3] Volatiles fractionate when magmas degas, such that insoluble volatiles are lost more rapidly than the more soluble species [*Burnard*, 2001; *Jambon et al.*, 1986, 1985; *Marty and Zimmerman*, 1999; *Sarda and Moreira*, 2002; *Moreira and Sarda*, 2000]. Experimental work has established that noble gas solubility decreases with increasing atomic mass [*Carroll and Stolper*, 1993; *Jambon et al.*, 1986; *Lux*, 1987]. Helium is more soluble than Ar, therefore He/Ar in magma should increase as the volatile concentration of the magma decreases due to degassing. The He-Ar system is particularly useful for examining magmatic degassing systematics as a) there is a large (factor of 10) difference in their solubilities and b) the $^4He/^{40}Ar$ ratio of the mantle is comparatively well constrained at between 2 and 4 [*Allègre et al.*, 1986].

[4] Recent work has shown that $^4He/^{40}Ar^*$ ($^{40}Ar^*$ is ^{40}Ar corrected for atmospheric contamination) of oceanic basaltic glasses worldwide increase as the He content of the basalt *increases*, the opposite to that predicted by solubility related degassing models [*Honda and Patterson*, 1999; *Matsuda and Marty*, 1995]. If degassing was the primary control on the magmatic $^4He/^{40}Ar^*$ ratio, the opposite trend would be expected, with high $^4He/^{40}Ar^*$ ratios in degassed basalts. While magmatic degassing must affect the He/Ar ratio trapped in basaltic glasses, this does not seem to be the dominant control. Variability of He/Ar ratios in MORB glasses have instead been attributed to high He diffusivities relative to Ar. In one such model, He (but not Ar) preferentially diffuses out of mantle minerals into melt pockets, resulting in high magmatic He/Ar ratios associated with high He abundances [*Fisher*, 1997; *Matsuda and Marty*, 1995]. In an alternative model, He and Ar are not fractionated from the mantle source ratio in the primary mantle melts, but, as the magma crystallizes, Ar is trapped in crystallizing phases, whereas He diffuses out of crystals back into the melt. As a consequence, He/Ar ratios and He contents are expected to increase with magmatic differentiation [*Honda and Patterson*, 1999]. The He/Ar ratios are further modified (in both models) by solubility controlled fractionation. Extensive

He loss, either preeruptive, syneruptive, or posteruptive, would also result in the trends observed; He diffusivities in basaltic glasses are high [*Kurz and Jenkins*, 1981] and posteruptive He loss from these samples is possible. In summary, it is not possible to model the absolute and relative He, Ne and Ar abundances of MORB glasses as either a diffusive processes or a solubility-controlled process: instead, both kinetic and equilibrium fractionation must occur at some point during transport of noble gases from their mantle source to the Earth's surface.

[5] Volatile compositions in basaltic glasses are also affected by magmatic degassing; magmatic degassing must produce an overprint on any fractionation that occurs due to He diffusion during either melting or crystallization as outlined above. Partly as a result of this degassing "overprint" obscuring more deep-seated processes, it is not possible to determine the primary control on relative noble gas abundances in basaltic glasses based on the currently available data. Furthermore, it will not be possible to determine the process – or processes – that control noble gas abundances in the sub-oceanic mantle unless the effects of magmatic degassing can be quantified.

1.2. Atmospheric Contamination

[6] Contamination of basaltic glasses by atmospheric noble gases is a well-recognised problem [*Ballentine and Barfod*, 2000; *Patterson et al.*, 1990; *Harrison et al.*, 2002]. Less well established, however, is the mechanism by which this contamination occurs. The atmospheric component found in certain gas-rich basaltic glasses (both MORBs and OIBs) is not associated with the release of magmatic He [*Ballentine and Barfod*, 2000; *Jambon et al.*, 1985]: magmatic and atmospheric noble gases are physically separated in these samples. Furthermore, relative noble gas abundances of the contaminant were consistent with contamination by unfractionated air, in contrast to the fractionated compositions expected of the seawater or subglacial ponds into which the basalts were intruded [*Moreira et al.*, 1998]. Ballentine and Barfod [*Ballentine and Barfod*, 2000] concluded that the atmospheric contaminant was added to the glasses after the glasses had chilled on the seafloor, and possibly only when the samples were exposed to air.

[7] Conversely, analyses of more typical, less gas-rich MORB glasses from both the Mid-Atlantic Ridge (MAR) and East Pacific Rise (EPR) than those examined by Ballentine and Barfod show that the amounts of ^{4}He and ^{36}Ar released by crushing are correlated [*Fisher*, 1997]. *Fisher* [1997] concluded that atmospheric and magmatic noble gases were both sited within vesicles in the glass. This requires addition of atmospheric noble gases to the magma itself. Alteration of oceanic crust by ^{36}Ar-rich hydrothermal fluids results in high concentrations of ^{36}Ar in altered portions of the crust. Fisher proposed that assimilation of altered crust by the ascending magma could result in atmospheric ^{36}Ar located within vesicles. Marty and Zimmerman [*Marty and Zimmerman*, 1999] developed this into a combined assimilation – fractional crystallization – degassing model where simultaneous crystallization and degassing was accompanied by introduction of ^{36}Ar through assimilation of crust.

2. Sample Locations and Descriptions

[8] The samples analyzed in this study were collected by dredge and rock chipper from three segments on the Mid-Atlantic Ridge (MAR). Five samples collected by dredging and by rock chipper from segment 8 (AMK3376 AMK3377 AMK3373 AMK3378 AMK3380) cover the entire length of the segment (25°40′N–25°80′N) with an average sample spacing of ≈10 km. Three rock chipper samples (AMK3410, AMK3412, AMK3413) are from the center and southern end of Segment 10 (26°10′N–26°35′N) while three further samples were collected by submersible and chipper from the center and southern tip of Segment 17 (AMK3427, AMK3339, AMK3351). Ridge depths were between 3000 and 4000 m below sea level (mbsl).

[9] All samples were clean, fresh glasses collected from neovolcanic zones within the MAR. Major and trace element compositions are available for samples 3351, 3339 and 3427 (Table 1). These show that these samples are typical depleted, relatively undifferentiated MORBs with low SiO2

Table 1. Sample Locations and Selected Major Element Compositions

Sample	Lat (N)	Long (W)	Depth (mbsl)	Seg	SiO_2	TiO_2	Al_2O_3	Fe_2O_3	FeO	MnO	MgO	CaO	Na_2O	K_2O	P_2O_5	SO_3	TOTAL	$^{87}Sr/^{86}Sr$
AMK3339	29:09	43:11		17	50.17	1.243	14.73	10.98	10.86	0.19	7.81	11.96	2.62	0.055	0.072	0.3	100.12	
AMK3351	29:08.68	43:10.57.	3143	17	49.52	1.241	14.89	10.89	10.77	0.16	7.77	12.09	2.64	0.067	0.077	0.28	99.64	0.702547 ± 8
AMK3373	25:40.86	45:08.45.	3987	8														
AMK3375	25:45.54	45:06.03	3468	8														
AMK3376	25:46.61	45:06.03.	3533	8														
AMK3377	25:48.35	45:05.29.	3404	8														
AMK3378	25:50.01	45:05.12.	3526	8														
AMK3380	25:54.49	45:02.55.	3832	8														
AMK3410	26:25.81	44:39.27	3438	10														
AMK3412	26:20.43	44:44.20	3661	10														
AMK3413	26:17.02	44:40.85	3825	10														
AMK3427	29:16.05	43:07.70	3230	17	49.66	1.355	14.77	10.98	10.86	0.18	7.61	11.8	2.81	0.093	0.114	0.29	99.65	0.702513 ± 7

(≈50%) and high MgO (7.5–8.2%). Sr isotopes have been measured on samples 3351 and 3427, and have typical MORB values of 0.7026.

3. Analytical Technique

[10] A new crushing apparatus was constructed in order to crush ≈1 gram samples of basaltic glass, yet maintain a low crusher blank. A schematic of the crusher is given in Figure 1. Coarse glass chips (mostly 3–5 mm) were ultrasonically cleaned in dilute HNO_3, de-ionized water then ethanol before loading into the crusher buckets. Ten samples were loaded onto a rotating carousel that permitted each sample to be crushed in turn without breaking vacuum; the crusher chamber was baked in ultra high vacuum for 24 hours at ≈150°C then allowed to pump for one week to ten days before starting analysis.

[11] Each sample was sequentially crushed by an external press, which could apply a pressure of up to 500 kg cm^{-2} (10,000 kg on a surface area of about 20 cm^2) (Figure 1), although only the final crushing steps required any appreciable pressure to be applied. The gases released by crushing were trapped on stainless steel sinter held at liquid N_2 temperature. Gases that would not condense on the steel sinter (essentially He, Ne and H_2) were purified on SAES NP10 getters (one at 250°C, another at room temperature) before analysis for He and Ne on a VG5400 magnetic sector mass spectrometer. The condensed gases were released off the sintered steel at 150°C and the amount of total volatiles released (assuming the noncondensable fraction to be minor) measured as a pressure change within a known volume of extraction system. Previous work has shown that it is likely that the gas released from vesicles in MORB glasses is predominantly (>90%) CO_2 [*Javoy and Pineau*, 1991] (technical difficulties prevented our usual procedure of checking the gas composition by quadrupole mass spectroscopy). Other contributions to the major gas phase are either considerably more soluble in basaltic melt than CO_2 (e.g., H_2O) or occur in trace amounts (SO_2, N_2 etc.) therefore are unlikely to affect the manometric CO_2 analyses at the ≈25% level of our accuracy. Also, at room temperature, water (if there

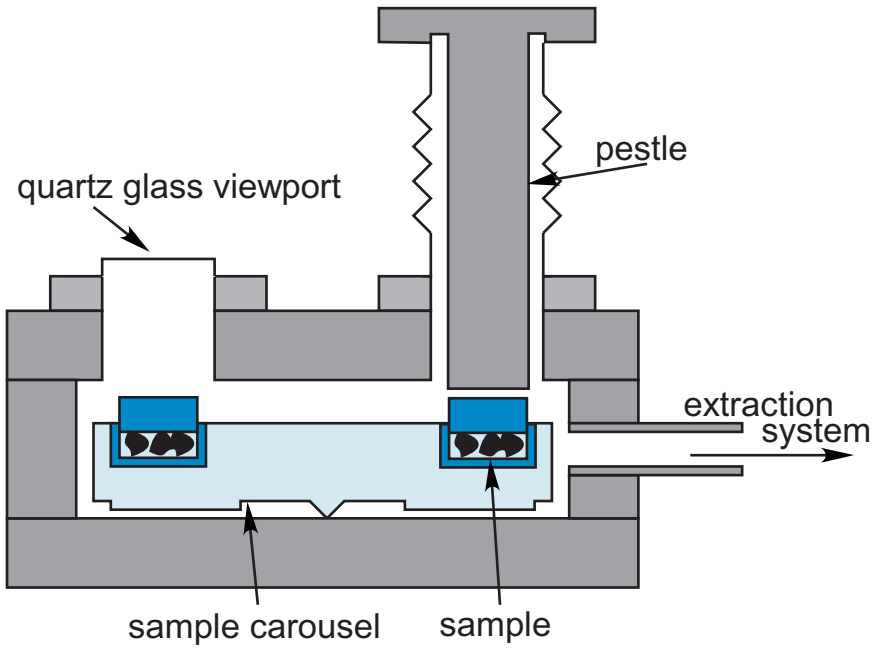

Figure 1. Schematic diagram of crusher. Approximately 1 g samples are loaded into small (25 mm diameter) stainless steel buckets that are placed in a circular stainless steel carousel (arrowed) that holds ten sample buckets. Pressure is applied to the sample through the stainless steel pestle. Once a sample has been completely crushed, the carousel is rotated to the next sample using a "wobble stick" mounted on the top flange (not shown); the carousel is aligned precisely using the quartz glass viewport. A dial gauge mounted on the pestle allowed the amount of sample compression that occurred during each step to be monitored precisely. Up to 10, 000 Kg could be applied to the pestle via an external hydraulic ram (not shown), corresponding to a pressure of up to 500 Kg cm^{-2} on the sample.

is any) contributes little to the pressure observed on the manometer; previous work has shown that the water condenses on the walls of the vacuum equipment (Manchester unpubl. data). After the gas was purified (using SAES getters), Xe was condensed on charcoal held at −110°C. Ar, then Xe (released off the charcoal at 120°C) were analyzed by the VG5400; Kr was not analyzed. Procedural blanks were monitored every day: careful vacuum practice ensured these were maintained below 0.1×10^{-9} cm^3 STP ^{40}Ar and 1×10^{-12} cm^3 STP ^{20}Ne; Xe blanks were below detection ($\approx 8 \times 10^{-15}$ cm^3 STP ^{132}Xe). ^4He blanks were variable, usually starting out below detection ($<10 \times 10^{-12}$ cm^3 STP) but as crushing progressed, the He blank increased up to 5×10^{-9} cm^3 STP, although this was still small (typically <1%) in comparison to the analyses.

[12] The mass spectrometer was calibrated against an internal standard consisting of air Ne, Ar, Kr and Xe but with added He such that $^4He/^{40}Ar$ (of the calibration gas) was 1.29 with $^3He/^4He = 5.9 \times 10^{-5}$. While He and Ne were not cryogenically separated for these measurements, the manufactured calibration gas ensured that the He/Ne ratio of the calibrations closely matched those of the samples. Note that the errors quoted do not rely purely on the counting statistics of the individual analysis, but also include the 1σ distribution of ten (or more) calibrations.

[13] The crushers did not completely crush the samples; after crushing, typically several glass chips remained ≤0.5 mm in size. After crushing, the samples were extracted from their buckets (not a totally trivial task as the press tended to compact the samples into a hard "pill" at the base of the bucket) and sieved through a 100 μm sieve: the proportion of glass crushed to <100 μm is given in Table 2.

4. Results

[14] Fourteen basalt glasses were step-crushed between 3 and 9 times per sample, depending on the gas content of the sample. The results reported

Table 2a. Noble Gas Concentrations

Sample	Crush	Weight (g)	>100 μm (g)	$^{4}He \times 10^{-6}$ (ccSTP)	$^{20}Ne \times 10^{-12}$ (ccSTP)	$^{40}Ar \times 10^{-6}$ (ccSTP)	$^{132}Xe \times 10^{-15}$ (ccSTP)	$CO_2 \times 10^{-6}$ (ccSTP)
AMK3376	1			0.33	17	0.053	n.m.	n.m.
	2			2.34	23	0.310	62	43
	3			3.35	46	0.469	119	61
	4			4.96	50	0.703	136	89
	5			1.44	30	0.127	40	23
	6			6.80	862	0.890	353	109
	7			2.36	141	0.340	2402	31
	8			0.41	23	0.038	b.d.	5
	9			0.19	51	0.056	47	9
	Total	**0.884**	**n.m.**	**22.19**	**1244**	**2.987**	**3159**	**369**
AMK3339	1			0.029	0	0.006	20	b.d.
	2			0.039	0	0.007	16	b.d.
	3			0.35	7	0.061	25	1
	4			0.59	10	0.094	42	1
	Total	**0.75**	**n.m.**	**1.01**	**16**	**0.168**	**103**	**2**
AMK3377	1			0.25	3	0.048	13	1
	2			0.57	7	0.111	26	2
	3			3.35	39	0.693	89	12
	Total	**0.516**	**n.m.**	**4.16**	**50**	**0.852**	**128**	**15**
AMK3351	1			0.95	35	0.144	71	10
	2			2.03	31	0.287	124	20
	3			1.69	24	0.229	98	12
	Total	**0.712**	**0.5528**	**4.67**	**90**	**0.661**	**294**	**42**
AMK3373	1			0.80	35	0.297	208	13
	2			1.41	21	0.457	80	23
	3			0.94	0	0.262	55	15
	4			0.29	9	0.078	26	1
	Total	**0.406**	**0.3011**	**3.44**	**65**	**1.095**	**370**	**51**
AMK3375	1			0.95	11	0.192	42	13
	2			6.02	64	1.039	231	76
	3			5.41	63	0.787	189	55
	Total	**0.851**	**0.6223**	**12.38**	**137**	**2.018**	**462**	**144**
AMK3378	1			0.27	2	0.052	b.d.	2
	2			1.80	16	0.328	42	14
	3			3.11	36	0.568	62	16
	Total	**0.739**	**0.5536**	**5.19**	**54**	**0.949**	**103**	**32**
AMK3380	1			0.56	5	0.097	17	5
	2			2.68	22	0.403	83	19
	3			0.91	11	0.095	35	2
	Total	**0.932**	**0.7104**	**4.15**	**39**	**0.595**	**136**	**25**
AMK3410	1			1.16	11	0.192	43	15
	2			5.91	57	0.899	205	84
	3			2.24	19	0.321	73	24
	Total	**0.6781**	**0.5025**	**9.31**	**86**	**1.412**	**320**	**123**
AMK3412	1			1.02	9	0.182	47	11
	2			4.30	46	0.733	169	26
	3			2.88	32	0.399	102	23
	Total	**0.761**	**0.5715**	**8.20**	**86**	**1.314**	**319**	**61**
AMK3413	1			2.58	27	0.382	50	b.d.
	2			5.90	66	0.828	135	b.d.
	3			2.88	54	0.360	84	25
	Total	**0.846**	**0.6341**	**11.36**	**148**	**1.570**	**269**	**25**
AMK3427	1			0.58	5	0.062	b.d.	2
	2			n.m.	36	0.203	34	8
	3			2.28	32	0.228	43	8
	Total	**0.623**	**0.5286**	**2.86**	**73**	**0.493**	**77**	**18**

Table 2b. Isotopic Compositions of Measured Gases

TITLE		$^{3}He/^{4}He$ Ra	$^{20}Ne/^{22}Ne$	$^{21}Ne/^{22}Ne$	$^{40}Ar/36Ar$	$^{129}Xe/^{132}Xe$	$^{132}Xe/^{130}Xe$
AMK3376	1	8.3 ± 0.4	8.5 ± 0.8	0.036 ± 0.009	609 ± 6	b.d.	b.d.
	2	8.7 ± 0.3	b.d. ±	b.d.	13884 ± 508	1.19 ± 0.06	7.0 ± 1.2
	3	8.1 ± 0.3	11.8 ± 1.1	0.043 ± 0.004	8617 ± 388	1.02 ± 0.04	6.5 ± 0.6
	4	7.7 ± 0.3	12.8 ± 1.2	0.060 ± 0.004	18187 ± 3842	1.11 ± 0.06	6.4 ± 0.7
	5	n.m.	11.4 ± 1.1	b.d.	5605 ± 135	1.06 ± 0.10	7.7 ± 2.1
	6	n.m.	10.6 ± 1.2	0.0280 ± 0.0004	1105 ± 30	1.02 ± 0.03	6.2 ± 0.4
	7	n.m.	10.0 ± 1.0	0.028 ± 0.001	646 ± 2	0.99 ± 0.02	6.8 ± 0.2
	8	n.m.	10.0 ± 0.9	0.041 ± 0.004	3804 ± 309	b.d.	b.d.
	9	n.m.	9.0 ± 0.9	0.030 ± 0.002	2641 ± 68	0.96 ± 0.14	7.8 ± 2.5
	Total	n.m.					
AMK3339	1	n.m.	b.d.	b.d.	1364 ± 39	1.05 ± 0.24	b.d.
	2	9.8 ± 0.9	b.d.	b.d.	1994 ± 58	1.16 ± 0.20	b.d.
	3	9.4 ± 0.4	b.d.	b.d.	5907 ± 311	1.14 ± 0.14	4.0 ± 1.4
	4	9.3 ± 0.4	b.d.	b.d.	6780 ± 665	1.03 ± 0.21	6.9 ± 2.5
	Total	**9.2 ± 0.4**					
AMK3377	1	9.4 ± 0.4	b.d.	b.d.	8065 ± 733	0.99 ± 0.20	b.d.
	2	8.9 ± 0.3	b.d.	b.d.	12736 ± 399	0.71 ± 0.17	b.d.
	3	8.5 ± 0.3	11.8 ± 1.1	0.047 ± 0.002	15471 ± 448	1.06 ± 0.06	7.1 ± 0.3
	Total	**8.6 ± 0.3**					
AMK3351	1	8.7 ± 0.2	8.9 ± 0.8	b.d.	3618 ± 82	0.90 ± 0.11	7.4 ± 1.7
	2	8.5 ± 0.2	9.1 ± 0.8	b.d.	5908 ± 367	1.00 ± 0.04	7.3 ± 0.4
	3	8.3 ± 0.2	b.d.	b.d.	8235 ± 180	1.07 ± 0.05	7.1 ± 0.8
	Total	**8.5 ± 0.2**	b.d. ±				
AMK3373	1	8.0 ± 0.2	9.1 ± 0.9	b.d.	1633 ± 14	1.05 ± 0.04	6.2 ± 0.2
	2	8.1 ± 0.2	b.d.	b.d.	24240 ± 696	1.09 ± 0.07	5.8 ± 0.4
	3	7.7 ± 0.2	b.d.	b.d.	19656 ± 936	1.03 ± 0.08	7.5 ± 1.0
	4	8.3 ± 0.2	b.d.	b.d.	6041 ± 167	0.93 ± 0.12	b.d.
	Total	**7.9 ± 0.2**					
AMK3375	1	8.1 ± 0.2	b.d.	b.d.	19863 ± 1242	1.05 ± 0.15	6.3 ± 0.9
	2	8.1 ± 0.5	13.0 ± 1.3	0.062 ± 0.003	16599 ± 349	1.09 ± 0.05	7.3 ± 0.5
	3	8.1 ± 0.5	13.3 ± 1.4	0.050 ± 0.005	10703 ± 234	1.18 ± 0.05	6.1 ± 0.3
	Total	**8.1 ± 0.5**					
AMK3378	1	8.1 ± 0.7	b.d.	b.d.	16117 ± 375	b.d.	b.d.
	2	8.7 ± 0.6	b.d.	b.d.	21693 ± 543	0.96 ± 0.14	5.6 ± 1.3
	3	8.4 ± 0.6	13.0 ± 1.2	0.053 ± 0.005	10269 ± 2055	1.15 ± 0.19	4.7 ± 0.6
	Total	**8.5 ± 0.6**					
AMK3380	1	8.2 ± 0.6	b.d.	b.d.	26219 ± 5244	1.32 ± 0.40	b.d.
	2	8.5 ± 0.6	12.7 ± 1.3	b.d.	24272 ± 2163	1.08 ± 0.08	6.1 ± 0.7
	3	7.9 ± 0.5	b.d.	b.d.	5375 ± 224	1.17 ± 0.18	4.7 ± 0.6
	Total	**8.3 ± 0.6**					
AMK3410	1	7.8 ± 0.5	b.d.	b.d.	23656 ± 2151	1.02 ± 0.14	6.1 ± 1.4
	2	7.9 ± 0.5	11.9 ± 1.2	0.053 ± 0.008	18745 ± 2884	1.06 ± 0.08	7.0 ± 0.4
	3	8.7 ± 0.6	b.d.	b.d.	19363 ± 1291	0.97 ± 0.16	8.2 ± 1.4
	Total	**8.1 ± 0.5**					
AMK3412	1	8.7 ± 0.6	b.d.	b.d.	17028 ± 2349	1.00 ± 0.09	6.0 ± 0.9
	2	8.3 ± 0.6	13.1 ± 1.3	0.051 ± 0.007	20688 ± 4310	1.04 ± 0.06	7.0 ± 0.7
	3	7.6 ± 0.5	11.3 ± 1.0	b.d.	15040 ± 627	1.09 ± 0.08	6.2 ± 0.6
	Total	**8.1 ± 0.5**					
AMK3413	1	7.5 ± 0.5	b.d.	b.d.	14011 ± 682	1.19 ± 0.12	b.d.
	2	8.0 ± 0.5	13.3 ± 1.3	0.053 ± 0.002	18003 ± 391	1.13 ± 0.07	7.3 ± 0.6
	3	7.7 ± 0.5	12.0 ± 1.1	0.050 ± 0.007	5285 ± 58	0.98 ± 0.17	7.2 ± 1.4
	Total	**7.8 ± 0.5**	b.d.				
AMK3427	1	8.0 ± 0.6	b.d.	b.d.	b.d.	b.d.	b.d.
	2	n.m.	12.1 ± 1.2	0.046 ± 0.003	11625 ± 564	1.23 ± 0.14	b.d.
	3	7.7 ± 0.5	11.4 ± 1.1	0.049 ± 0.009	11191 ± 405	1.08 ± 0.17	4.4 ± 0.8
	Total	**7.7 ± 0.5**					

n.m., not measured; b.d., below detection. >100 μm refers to the fraction of the sample that would not fit thorugh a 100 μm seive after crushing.

here are not blank corrected; the analyses are considered to lie on a mixing line between an air-derived component and a mantle component. With the exception of He, blanks were isotopically indistinguishable from air, therefore blank correcting the data simply shifts the analyses along the air-mantle mixing line. The uncertainty added by blank correcting the data is not warranted by the minor shift along a well-established correlation.

[15] The results are given in Table 2. Total gas contents ranged from 5 to 25 μcc ^{4}He g^{-1}. There is no relation between noble gas composition (either isotopic or relative abundances) and the amount of gas preserved in that sample. With the exception of the He isotopic composition (which clustered around the MORB average of 8.5), there was a broad range in elemental and isotopic compositions in the released gases. ^{20}Ne/^{22}Ne, ^{40}Ar/^{36}Ar and ^{129}Xe/^{130}Xe ranged from compositions close to the atmospheric ratio to significantly higher values (13.3 ± 1.3, 26, 000 ± 6000 and 8.3 ± 0.6 respectively). The highest (least air-like) ratios are most common in the latter crushing steps. Radiogenic isotope ratios such as ^{4}He/^{40}Ar* and ^{21}Ne*/^{4}He are also variable (2.7–11.4 and (0.7–3.5) × 10^{-8} respectively), with variation within multiple crushes of individual samples and from sample to sample. (The asterisk indicates corrected for atmospheric contamination assuming ^{36}Ar is atmospheric in origin and the ^{20}Ne/^{22}Ne ratio of the mantle is 13.8 with a primordial ^{21}Ne/^{22}Ne of 0.0032 using the formula given by *Honda et al.* [1993].).

[16] The narrow sampling interval on Segment 8 allows variations in noble gas concentrations and isotopic compositions within a single segment to be examined. Although AMK3376 (the most gas-rich sample in the suite) is from the center of Segment 8, there is no other evidence that higher magmatic productivity in the center of the ridge segment leads to higher volatile concentrations. Samples adjacent to AMK3376 – and still close to the center of the segment – do not have high volatile concentrations. Isotopic compositions (^{40}Ar/^{36}Ar, ^{3}He/^{4}He) also appear to be independent of sample location with respect to ridge segmentation.

5. Discussion

[17] The variations in noble gas isotope compositions (e.g., ^{20}Ne/^{22}Ne, ^{40}Ar/^{36}Ar and ^{129}Xe/^{132}Xe) and in relative noble gas abundances (e.g., ^{21}Ne*/^{4}He, ^{40}Ar*/^{4}He) are not likely to represent variations in the MORB mantle, which is thought to be relatively well mixed and homogeneous with respect to the noble gases [*Allègre et al.*, 1986]. Rather, these variations reflect shallow level processes that have modified the compositions of the mantle-derived volatiles. Principle among these are air-contamination and noble gas fractionation during magmatic degassing, although the order that these processes operated is not known.

5.1. Air Contamination

[18] There are good correlations between ^{20}Ne/^{22}Ne and ^{21}Ne/^{22}Ne, ^{40}Ar/^{36}Ar, CO_2/^{36}Ar and ^{129}Xe/^{132}Xe (Figures 2a–2d) and ^{129}Xe/^{130}Xe and ^{132}Xe/^{130}Xe (not shown), all of which are consistent with contamination of mantle-derived volatiles that have high ^{20}Ne/^{22}Ne, ^{21}Ne/^{22}Ne, ^{40}Ar/^{36}Ar, ^{129}Xe/^{130}Xe and ^{132}Xe/^{130}Xe ratios with an air derived contaminant (ADC) with atmospheric, or near-atmospheric, compositions of the above isotope ratios. However, the relative noble gas abundances of the ADC (Ne/Ar, Xe/Ar etc.) are not necessarily atmospheric: if the contaminating agent was seawater rather than air (for example), then the ADC would have atmospheric ^{20}Ne/^{22}Ne, ^{40}Ar/^{36}Ar and ^{129}Xe/^{130}Xe, but higher Ar/Ne and Xe/Ne than air due to the greater solubility of Ar and Xe than Ne in water [*Ballentine and Barfod*, 2000; *Harrison et al.*, 2002; *Patterson et al.*, 1990]. *Harrison et al.* [2002] have shown that Icelandic basalts were contaminated by an ADC with Xe/Ne ≫ air in addition to unfractionated air, demonstrating the complexities of atmospheric noble gas contamination.

[19] The effects of the air-derived contaminant can be deconvolved using Ne isotopes. Neon has three isotopes, ^{20}Ne, ^{21}Ne and ^{22}Ne: ^{21}Ne is the only one produced in significant quantities in the mantle, primarily by α-particle reactions with oxygen. The ^{20}Ne/^{22}Ne ratio of the mantle (≥12.5) is significantly higher than that of the atmosphere (^{20}Ne/^{22}Ne = 9.8) [*Moreira et al.*, 1998; *Sarda et*

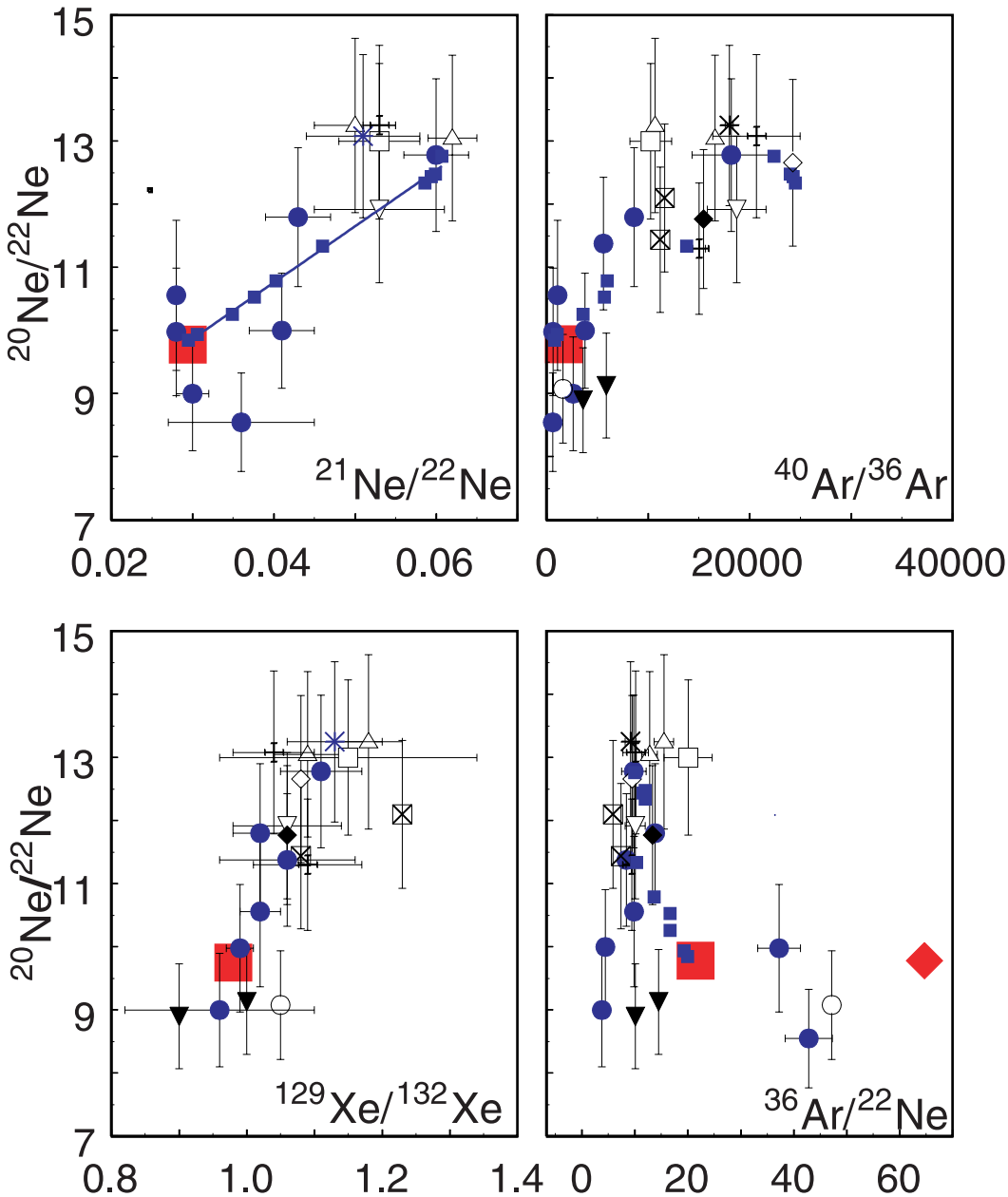

Figure 2. $^{20}Ne/^{22}Ne$ versus air affected isotopes such as $^{21}Ne/^{22}Ne$, $^{40}Ar/^{36}Ar$, $CO_2/^{36}Ar$, $^{129}Xe/^{132}Xe$, $^{36}Ar/^{22}Ne$. $^{20}Ne/^{22}Ne$ versus $^{36}Ar/^{22}Ne$, AMK data (AMK3376, filled circle; AMK3339, filled square; AMK3377, filled diamond; AMK3351, filled triangle; AMK3373, open circle; AMK3375, open up triangle; AMK3378, open square; AMK3380, open diamond; AMK3410, open down triangle; AMK3412, cross; AMK3427, X square; AMK3413, star) and popping rock (small solid squares, data of Moreira). Both data sets are consistent with mixing between magmatic gases with $^{20}Ne/^{22}Ne \geq 12.5$ and an air-derived contaminant (ADC) with $^{20}Ne/^{22}Ne$ indistinguishable from air (= 9.8). In the case of popping rock, $^{36}Ar/^{22}Ne$ of the ADC appears to be nearly constant and is compatible with that of air (= 18) whereas the ADC in the AMK glasses is highly variable, with $^{36}Ar/^{22}Ne$ ratios both lower than air (e.g., AMK3427) and higher than air (e.g., AMK3373). $^{129}Xe/^{132}Xe$ is plotted in preference to $^{129}Xe/^{130}Xe$ as the low abundances of ^{130}Xe results in large errors.

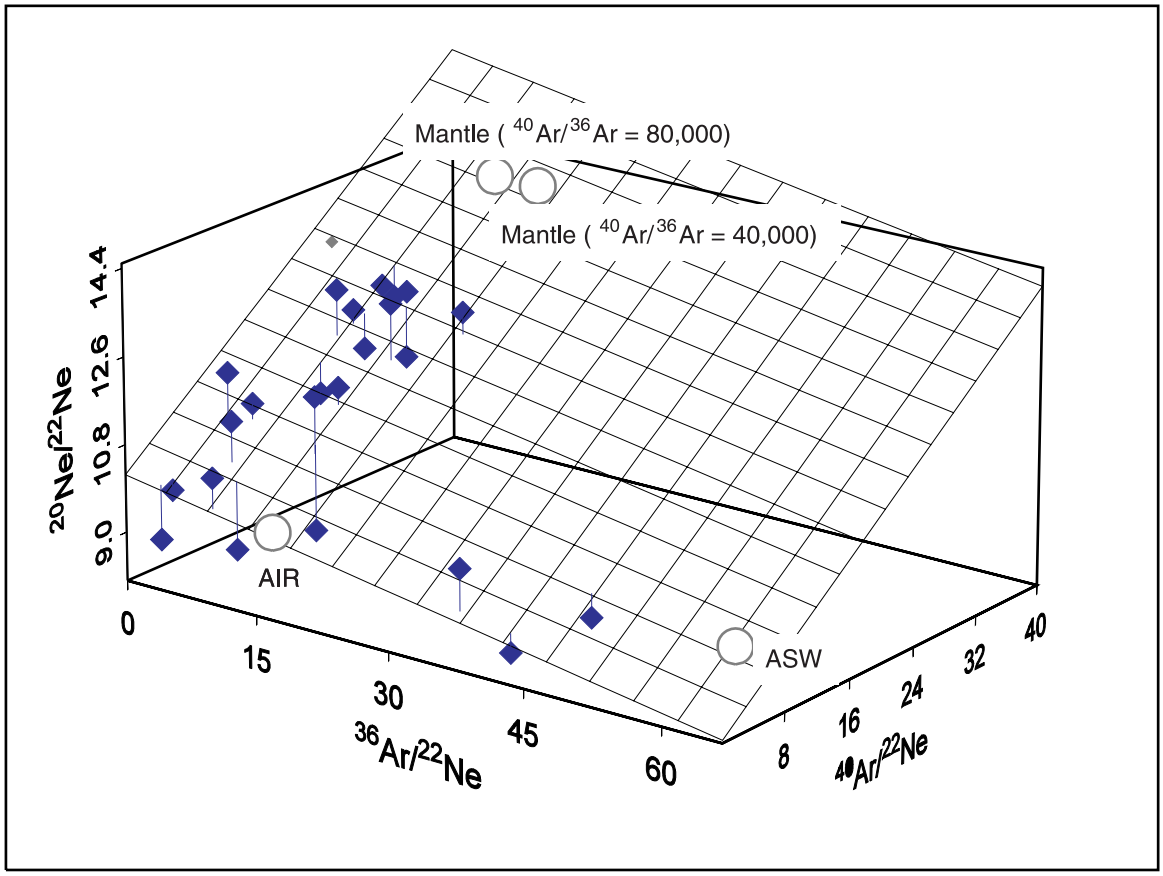

Figure 3. "Turnery" diagram (3D $^{20}Ne/^{22}Ne$ - $^{36}Ar/^{22}Ne$ - $^{40}Ar/^{22}Ne$ discrimination plots). All AMK samples, this study (individual crush steps not distinguished for clarity). The data lie on a plane as opposed to a line, indicating that the noble gases present in these samples are mixtures of three or more distinct components. The mantle $^{40}Ar/^{36}Ar$ cannot be constrained without first constraining the mantle $^{36}Ar/^{22}Ne$ ratio [*Harrison et al.*, 2001]. Mixing lines for binary mixing between air and mantle noble gases with $^{40}Ar/^{36}Ar$ = 40, 000 (dashed line) and $^{40}Ar/^{36}Ar$ = 80, 000 (solid line) are shown for reference ($^{36}Ar/^{22}Ne$ = 11.8 and 5.9, respectively). The AMK data define a plane that is more steeply dipping than that of the popping rock data with higher Ar/Ne for a given $^{20}Ne/^{22}Ne$ ratio (see also Figure 2d). The high Ar/Ne ratios of the AMK suite are likely due to volatile fractionation during gas loss from the magma.

al., 1988; *Trieloff et al.*, 2000]. The $^{20}Ne/^{22}Ne$ ratio is essentially unaffected by nuclear processes and therefore the slope of a line in a $^{20}Ne/^{22}Ne$ – $^{21}Ne/^{22}Ne$ plot is independent of atmospheric contamination and characteristic of the sample $^{21}Ne/^{22}Ne$ ratio. The slope of the $^{20}Ne/^{22}Ne$ – $^{21}Ne/^{22}Ne$ correlation is consistent with previous analyses that show that the MORB $^{21}Ne/^{22}Ne$ ratio extrapolated to a $^{20}Ne/^{22}Ne$ ratio of 13.8 is ≈0.07 [*Moreira et al.*, 1998; *Sarda et al.*, 1988].

[20] On a local scale, $^{20}Ne/^{22}Ne$ and other air-affected isotope ratios (such as $^{40}Ar/^{36}Ar$ or $^{129}Xe/^{130}Xe$) also correlate, because both ratios are a function of the same process, the addition of air-derived to mantle-derived noble gases [*Farley and Poreda*, 1993; *Moreira et al.*, 1998]. However, plotting two independently varying isotope ratios on two axes results in a series of hyperbolae, each of which represents a range in end-member compositions. It is preferable to use a four-isotope system using 3-D "Turnery" diagrams (see *Harrison et al.* [2002] for a more detailed discussion).

[21] The AMK glass compositions define a plane in a $^{20}Ne/^{22}Ne$-$^{36}Ar/^{22}Ne$-$^{40}Ar/^{22}Ne$ "Turnery diagram" (Figure 3), therefore these compositions must result from a mixture of at least three components. Contamination of magmatic gases by either air alone or air saturated water (ASW) alone

would result in a linear data array, as opposed to the plane observed. The AMK glasses have been contaminated by air-derived noble gases with a range in $^{36}Ar/^{22}Ne$. Unlike the glasses examined by Ballentine and Barfod (see section 1 and *Ballentine and Barfod* [2000]), the dominant contaminant for the AMK glasses is *not* unfractionated air; plotting the data on the same discrimination diagram as *Ballentine and Barfod* [2000] (Figure 2d), it is clear that the Ar/Ne in the ADC end-member is considerably more variable in the AMK samples than in gas rich basaltic glasses such as "popping rock" or DICE glass [*Ballentine and Barfod*, 2000].

[22] Most aqueous fluids have $^{36}Ar/^{22}Ne >$ air; also air adsorbed onto the sample surface will have $^{36}Ar/^{22}Ne >$ air. Therefore, atmospheric contaminants will likely have $^{36}Ar/^{22}Ne$ between that of air (18) and ASW (≈65). From Figures 2d and 3, it appears that $^{36}Ar/^{22}Ne$ of the ADC ranges between values greater than air ($^{36}Ar/^{22}Ne_{air} = 18$) but also values less than air (as low as 5). It is not immediately obvious how these basalts preferentially entrained air Ne relative to air Ar. Some tektites [*Matsubara and Matsuda*, 1991] and Icelandic glasses (P. Burnard, unpublished data, 1996) have Ar/Ne ratios $\ll$ air, attributed to preferential diffusion of atmospheric Ne (without Ar) into the glasses after impact melting (tektites) or eruption (glasses). It seems plausible that diffusion-in of atmospheric Ne may have resulted in the low Ne/Ar ratios in the ADC in these samples.

[23] The plane fitted to the Ne-Ar data from the AMK glasses is steeper than that of the "popping rock" data (Figure 3); these glasses have higher Ne/Ar ratios than the "popping rock" (for a given $^{20}Ne/^{22}Ne$). This is likely due to fractionation of Ne from Ar during degassing of the parent AMK magmas (see section 5.3). It is not possible to determine if atmospheric contamination predated volatile fractionation or vice versa: the predicted "Turnery" diagram trajectories for fractionation followed by contamination are the same as for contamination then fractionation.

[24] The $^{4}He/^{40}Ar^{*}$ ratios of these glasses is ~3 times the production ratio; considering that $S_{Ne}/S_{Ar} \approx 0.5 * S_{He}/S_{Ar}$ [*Carroll and Webster*, 1994], the Ne/Ar ratio of the basalts will be a maximum of 1.5 times higher than the undegassed magma. Assuming $^{36}Ar/^{22}Ne$ of the AMK magmas prior to degassing was ≈10 (i.e., the same as popping rock [*Moreira et al.*, 1998]), then the predicted $^{36}Ar/^{22}Ne$ ratio of the fractionated AMK magma would be ≈7, which is broadly consistent with the observed ratios.

[25] From Figure 2d, it is clear that there is a range in $^{36}Ar/^{22}Ne$ at any given $^{20}Ne/^{22}Ne$, especially at low $^{20}Ne/^{22}Ne$ ratios. In order that this occurs, contamination by atmospheric Ar without a constant addition of atmospheric Ne must occur in these samples. Estimating the mantle $^{36}Ar/^{22}Ne$ ratio by extrapolating to a given mantle-like $^{20}Ne/^{22}Ne$ ratio in Figure 2d will not adequately correct for addition of atmospheric Ar. Similarly, although there are well-defined relationships between $^{20}Ne/^{22}Ne$ and $^{40}Ar/^{36}Ar$ or $^{129}Xe/^{132}Xe$ (Figure 2), it is not possible to constrain the source region $^{40}Ar/^{36}Ar$ or $^{129}Xe/^{132}Xe$ without prior knowledge of the mantle $^{36}Ar/^{22}Ne$ or $^{132}Xe/^{22}Ne$ ratios [*Harrison et al.*, 2002].

[26] In summary, it appears likely that four or more components have contributed to the noble gas inventory trapped in these samples: (1) a magmatic component with Ar/Ne ratios higher than that of the mantle; (2) atmospheric Ne that has diffused into the samples without accompanying atmospheric Ar; (3) air; (4) an air saturated fluid with $Ar/Ne > (Ar/Ne)_{air}$. The complexities of mixing between these end-members means that little information on the mantle noble gas isotope ratios can be gleaned from these data other than they broadly support the conclusions of *Moreira et al.* [1998] and interpretation of their data by *Harrison et al.* [2002].

5.2. Contamination Mechanisms

[27] Assimilation of ^{36}Ar-bearing altered oceanic crust was proposed by *Fisher* [1997] (see section 1) based on correlations between $^{4}He/^{40}Ar^{*}$ and $^{36}Ar/^{40}Ar^{*}$ for multiple analyses (step crushing) of individual samples. However, in contrast to the observations of *Fisher* [1997], there is no clear

relation between $^{4}He/^{40}Ar^{*}$ and $^{36}Ar/^{40}Ar^{*}$ in multiple crush steps of individual glasses in this study (not shown); assimilation of ^{36}Ar bearing crust does not appear to have occurred in these basalts.

[28] The correlation between $^{4}He/^{40}Ar^{*}$ and $^{36}Ar/^{40}Ar^{*}$ observed in stepped crush data of several basaltic glasses (reported by *Fisher* [1997]) could be an artifact of the crushing technique: (1) The "slug" type of crushers (used in the study by [*Fisher*, 1997]) are likely to release air-derived ^{36}Ar during crushing due to the action of the iron "slug" on the vacuum chamber walls (extraction blanks with no sample are unlikely to mimic the abrasive action of glass powder on the crusher walls); and (2) $^{4}He/^{40}Ar^{*}$ increases in small vesicles (see below and *Burnard* [1999a]), and therefore $^{4}He/^{40}Ar^{*}$ will likely increase as crushing progressively fractures smaller and smaller vesicles [*Burnard*, 2001].

[29] Thus, the increase in ^{36}Ar produced by the crushing equipment used by *Fisher* [1997] with crushing duration, coupled with the change in He/Ar with vesicle size, can result in a fortuitous correlation between $^{36}Ar/^{40}Ar^{*}$ and $^{4}He/^{40}Ar^{*}$, as reported by [*Fisher*, 1997]. It seems unlikely, therefore, that crustal assimilation is a significant source of ^{36}Ar in oceanic basalts.

[30] Some of the AMK samples (but not all) have increasing $^{40}Ar/^{36}Ar$ with progressive crushing (Table 2). The high $^{40}Ar/^{36}Ar$ of later crushes of some samples is likely to be due to removal of a persistent contaminant, possibly adsorbed on the sample surface or located in microcracks, by the earlier crushing steps.

5.3. Volatile Fractionation During Degassing

[31] With the exception of sample AMK3373, all measured $^{4}He/^{40}Ar^{*}$ ratios are higher than reasonable production/accumulation values for the MORB mantle (i.e., between 2 and 4; see section 1). There also is a range of volatile compositions for each glass; $^{4}He/^{40}Ar^{*}$ and $^{4}He/CO_2$ systematically increase with progressive crushing (Figure 4). $^{40}Ar^{*}/CO_2$ generally decreases during crushing. These patterns are expected for solubility – determined magmatic degassing. The range in composition found in each sample likely results from rupturing progressively smaller vesicles as crushing progresses; the smallest vesicles in a basaltic glass sample nucleated last and preserve the most fractionated volatiles [*Burnard*, 2001, 1999a]. It should be noted that $^{4}He/^{40}Ar^{*}$ of the AMK samples are at the low – undegassed – end of the spectrum of compositions found in MORBs globally: $^{4}He/^{40}Ar^{*}$ values as high as 50 are commonly found in MORBs erupted at comparable depths to these samples [*Jambon et al.*, 1985; *Marty and Zimmerman*, 1999; *Sarda et al.*, 2000].

[32] The lack of a correlation between eruption depth and a degassing index (such as $^{4}He/^{40}Ar^{*}$) demonstrates that comparatively small variations in eruption pressure ($\leq$50 bars) do not affect the amount of magmatic degassing. This is perhaps unsurprising considering that CO_2 bubbles nucleate at considerable depth in the crust [*Pan et al.*, 1991]. The narrow range in $^{4}He/^{40}Ar^{*}$ in these samples suggests that magmas from this section of the MAR all degassed to more-or-less the same extent. Experimentally determined He and Ar solubilities suggest that, during distillation, loss of only 10–20% of the original volatiles would result in $^{4}He/^{40}Ar^{*} \approx 6–8$ (assuming an initial $^{4}He/^{40}Ar^{*}$ of 3), as observed in these samples. Alternatively, batch degassing (as opposed to distillation) may have produced the volatile fractionation seen in these samples. Two episodes of vesiculation would be required to account for the compositions in these samples, one of which was lost (resulting in a high He/Ar magma) while the second produced the vesicles that are analyzed in the glass. It is not possible to distinguish between batch and distillation degassing mechanisms with these data.

[33] Segments 8 and 10 have noticeably higher volatile concentrations and higher $^{40}Ar/^{36}Ar$ ratios than Segment 17, with a good relationship between eruption depth and $^{40}Ar/^{36}Ar$ (Figure 5). For example, the maximum $^{40}Ar^{*}$ of any Segment 17 sample is 0.6 μcc STP g^{-1}, while the minimum $^{40}Ar^{*}$ of all of the remaining

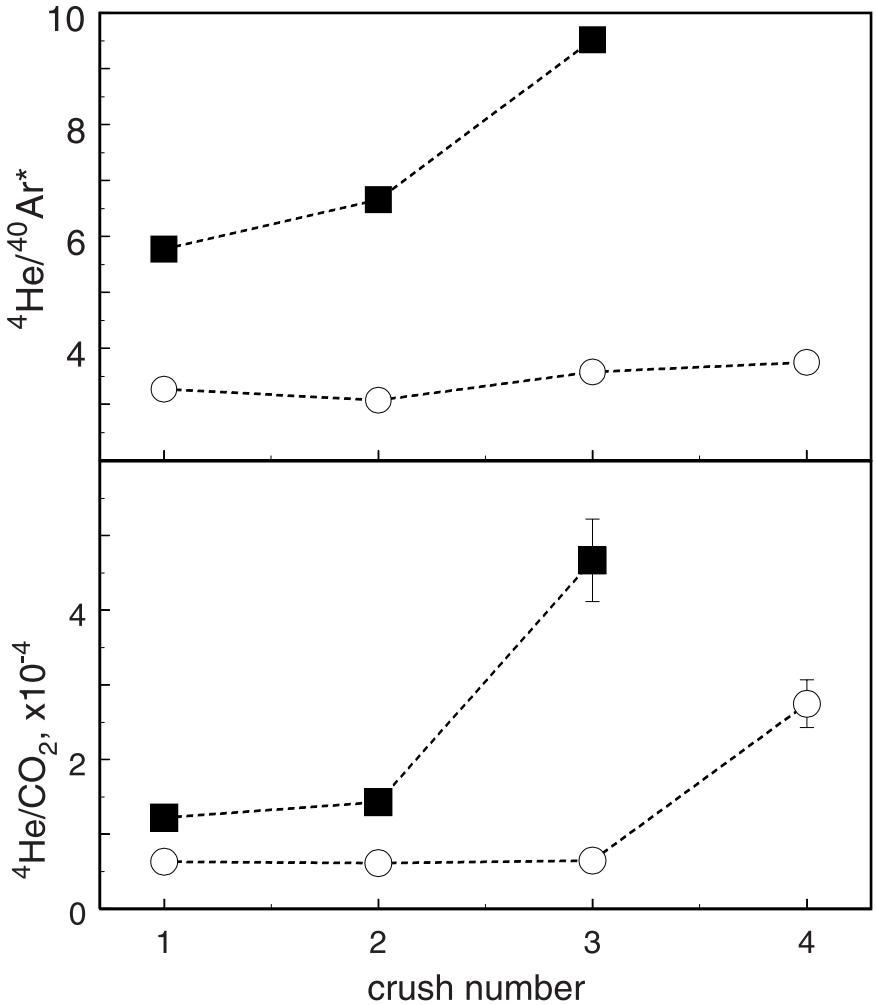

Figure 4. Variations within multiple crush steps of the same sample. $^4He/^{40}Ar$ (top) and $^4He/CO_2$ (bottom) against crush number for two representative AMK glasses. AMK3339, circles; AMK3380, squares. He/CO_2 increases as crushing progresses, particularly for the last crush of each sample. He/Ar increases also, although less rapidly than for He/CO_2. Given that the greatest differences in solubility are between He and Ar, the He-CO_2 fractionation is likely due to preferential CO_2 removal from the final crush steps, whereas He-Ar fractionation is due to fractional degassing.

samples is also 0.6 μcc STP g^{-1}; the average $^{40}Ar^*$ concentration of Segment 17 samples is a factor of three lower than the average of Segments 10 and 8. The low $^{40}Ar/^{36}Ar$ ratios are to be expected of samples that have low concentrations of magmatic gases, but it is not immediately obvious why the Segment 17 samples should have lower noble gas concentrations. At 3200 mbsl, Segment 17 is the most shallow of the segments sampled. Differences in internal vesicle pressure arising from the variation in eruption depths cannot account for the noble gas concentration variability, as the pressure differences are only 20%. However, the lower eruption pressure of Segment 17 glasses may determine the ability of the glasses to preserve their vesicles, as discussed in the following section.

5.4. Preservation of Volatiles in Basaltic Glasses

[34] The vast majority of magmatic volatiles are not preserved in basaltic glasses. For example, 1 gram of basalt glass (density ≈2.8 gcm^{-3}) has a typical vesicularity of 0.5–1%. [*Dixon et al.*, 1988; *Kurz and Jenkins*, 1981]; a nonquantitative inspection of thin sections of these glasses show that these vesicularities are within this range and occa-

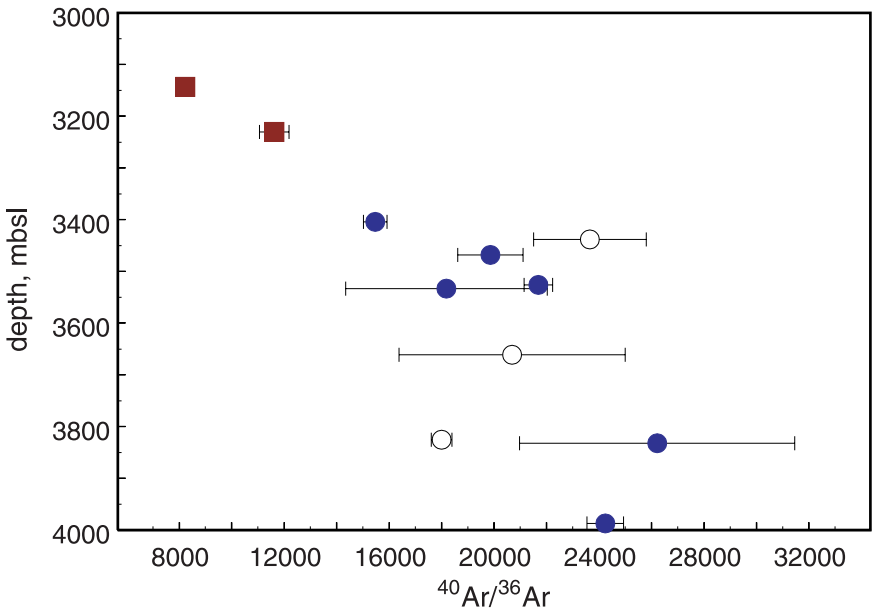

Figure 5. $^{40}Ar/^{36}Ar$ as a function of ridge depth. The maximum $^{40}Ar/^{36}Ar$ ratio measured on each sample is plotted against ridge depth at the sampling site (solid circles, Segment 8; open circles, Segment 10; solid squares, Segment 17). Despite a relatively small change in ridge depth, there is a clear relationship between $^{40}Ar/^{36}Ar$ and eruption depth, with high $^{40}Ar/^{36}Ar$ ratios (>15,000) limited to samples erupted at high pressure (i.e., under a greater column of seawater).

sionally higher. This vesicularity corresponds to $14–28 \times 10^{-3}$ cm^{-3} of vesicle volume per gram of glass. If all the vesicles were filled with magmatic volatiles (predominantly CO_2) at the eruption pressure (~300 bars), then MORB glasses would have CO_2 concentrations of 4–8 cm^3 STP CO_2 per gram of basaltic glass. Examination of Table 2 shows that 90% or more of the vesicles in the AMK samples are empty. Either the vesicles leaked (ruptured) after eruption, or they never trapped volatiles in the first place (e.g., they may be shrinkage features). Small variations in the amount of vesicles preserved will therefore have a dramatic effect on the amount of gas extracted from the sample during analysis. As a result, variations in noble gas content in different ridge sections may reflect vesicle preservation rather than magmatic or degassing phenomena.

[35] $^{4}He/^{40}Ar^*$ ratios are essentially indistinguishable in all segments, implying an approximately constant degree of magmatic degassing. At first glance, this is inconsistent with the low $^{40}Ar^*$ concentrations in Segment 17 samples. These observations can be reconciled if the depth of the ridge determines the amount of gas trapped or preserved in the glass but not the extent of gas lost from the magma. It seems most likely that degassing is essentially a magma chamber (as opposed to eruption) phenomenon, as concluded by *Marty and Zimmerman* [1999] and *Burnard et al.* [2002], whereas vesicle preservation is determined by eruption pressure.

[36] A trend of decreasing $^{40}Ar/^{36}Ar$ with increasing $^{206}Pb/^{204}Pb$ in Mid-Atlantic MORBs led *Sarda et al.* [1999] to conclude that atmospheric Ar was recycled to the mantle along with crustal (radiogenic) Pb. However, *Burnard* [1999b] suggested that the trend may be co-incidental: ridge segments with radiogenic Pb are more shallow than "normal" ridges, and therefore likely to be more degassed. Degassed samples will be more susceptible to atmospheric contamination and consequently have lower $^{40}Ar/^{36}Ar$ ratios, resulting in a relationship between Pb and Ar isotopes that is not due to the composition of the mantle source to the basalts. Although the change in ridge depth in this study is small (<1000 m in comparison to >3000 m in the Sarda et al. study),

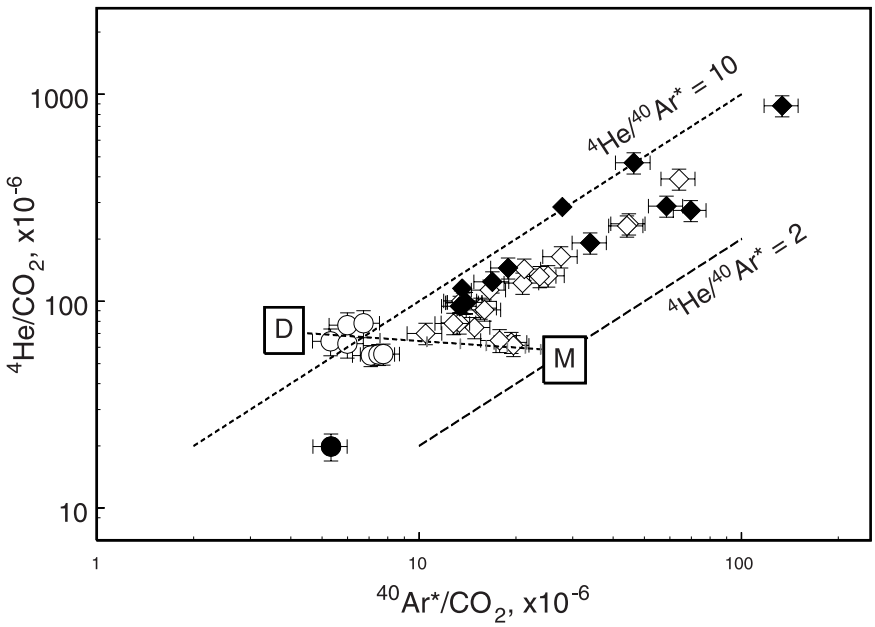

Figure 6. ^{4}He and ^{40}Ar concentrations in the volatile phase. AMK samples with data from more than one crush. Circles, AMK3376; Diamonds, remaining samples (individual samples not distinguished for clarity). The final crush steps of each sample are highlighted (solid symbols). Previous estimates of the "initial" (i.e., prior to any degassing) volatile compositions for MORB mantle melts is given by "M" [*Marty and Zimmerman*, 1999]; the line extending from "M" to lower $^{40}Ar^*/CO_2$ at near constant $^4He/CO_2$ is the predicted compositions resulting from equilibrium degassing of these volatiles. "D" is the composition predicted for a MORB magma that has lost 30% of its original volatiles (solubilities are from *Carroll and Webster* [1994]). It is clear that the range in noble gas concentrations in the volatile phase in these samples is much greater than the range in He/Ar that would result from equilibrium degassing. With the exception of AMK3376, the highest $^4He/CO_2$ and $^{40}Ar^*/CO_2$ values for each particular sample are from the last crush of that sample. The overall correlation results from variations between samples: multiple crushes of indivdual samples (with the exception of the last crush steps) are usually parallel to the degassing trend marked by the line M – D.

there is a clear relationship between $^{40}Ar/^{36}Ar$ and ridge depth (Figure 5), demonstrating that the primary control on the $^{40}Ar/^{36}Ar$ ratio of a basalt is not its' mantle source. However, in contrast to the Azores [*Moreira and Allègre*, 2002] and the Amsterdam-St Paul plateau [*Burnard et al.*, 2002], magmatic degassing cannot be the control on the $^{40}Ar/^{36}Ar$ ratio because all samples essentially have the same $^4He/^{40}Ar^*$ (with the exception of AMK3339). Instead, it is likely that vesicle preservation determines the concentration of magmatic Ar – and consequently the $^{40}Ar/^{36}Ar$ ratio – in these samples. Variable vesicle preservation with or without magmatic degassing could result in the relation between $^{40}Ar/^{36}Ar$ and $^{206}Pb/^{204}Pb$ reported by *Sarda et al.* [1999]. Irrespective of the cause, the fact that there are strong correlations between $^{40}Ar/^{36}Ar$ and eruption depth throws significant doubt on the plausibility of recycling atmospheric Ar to the MORB mantle source.

5.5. Noble Gas Concentrations in the Volatile Phase

[37] The noble gas:CO_2 ratio is equivalent to the concentration of noble gases in the volatile phase: while this assumes that the volatile phase (i.e., that trapped in the vesicles) is composed entirely of CO_2, major variations in the composition of the volatile phase (i.e., CO_2 fraction of the volatile phase $\ll$ 50%) would be required to affect the following discussion. Variations in noble gas concentration in the volatile phase ($\equiv$ noble gas/CO_2) are not subject to the same vesicle preservation problems as noble gas concentrations in a rock. There is a positive correlation between $^4He/CO_2$ and $^{40}Ar^*/CO_2$ for the dataset as a whole (Figure 6).

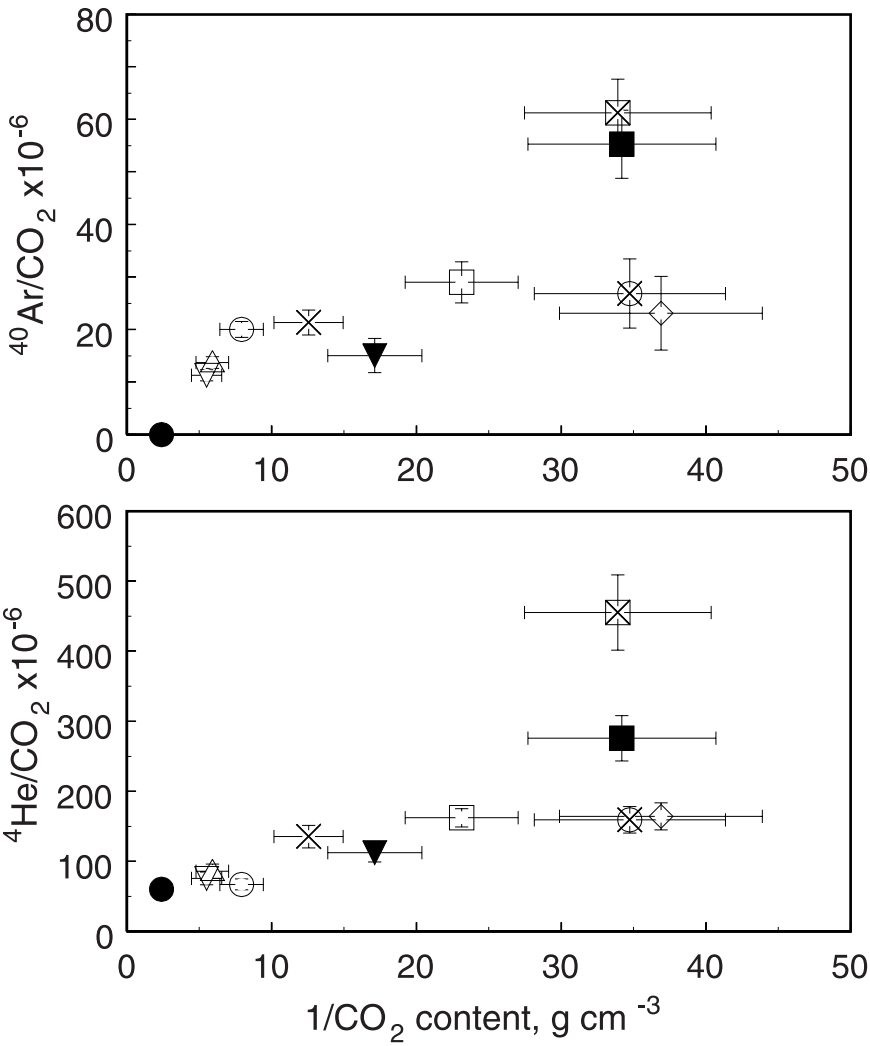

Figure 7. $^{40}Ar^*/CO_2$ and $^{4}He/CO_2$ as a function $1/[CO_2]$. Total data (i.e., sum of all crush steps) shown. AMK3376, filled circle; AMK3339, filled square; AMK3377, filled diamond; AMK3351, filled triangle; AMK3373, open circle; AMK3375, open up triangle; AMK3378, open square; AMK3380, open diamond; AMK3410, open down triangle; AMK3412, cross. There is a general inverse correlation between CO_2 concentration in the sample and noble gas/CO_2 ratio.

Also, the ^{4}He and ^{40}Ar concentrations in the volatile phase increase as the amount of volatiles trapped in the glass – i.e., the CO_2 concentration – decreases (Figure 7). The large range in He/CO_2 and Ar/CO_2, and the correlation between them, cannot be produced by solubility-controlled fractionation; solubility-controlled fractionation would result in a negative correlation between $^{4}He/CO_2$ and $^{40}Ar^*/CO_2$ ([*Burnard*, 2001] and Figure 6). The range in noble gas/CO_2 relative to the range in $^{4}He/^{40}Ar^*$ is considerably greater in these analyses than would be predicted by solubility-determined degassing of a single initial volatile composition. Some process or processes other than solubility-determined degassing appear to control noble gas concentrations in the volatile phase.

[38] Two separate effects need to be examined: (1) variation in He/Ar and He/CO_2 of individual crush steps of each sample and (2) range in, and correlation between, He/CO_2 and Ar/CO_2 of the entire dataset.

5.5.1. Variations Within Each Sample

[39] Most noble gas/CO_2 variation occurs in the last crush step of each sample (Figures 4 and 6). As

crushing progresses, $^4He/CO_2$ is approximately constant while $^{40}Ar^*/CO_2$ decreases (Figure 4), until the very last crush steps. These usually have high $^4He/CO_2$ and $^{40}Ar^*/CO_2$ (relative to the previous analyses). Either noble gas-CO_2 fractionation is most significant in the smallest vesicles (as sampled by the final crush steps) or else it is the crushing process itself that fractionates noble gases from CO_2.

[40] As sample grain size is reduced during crushing, CO_2 will be adsorbed on the fresh glass surfaces. Experiments by *Barker and Torkelson* [1975] have shown that the amount of CO_2 adsorbed by crushing quartz and basalt in vacuo was between 10 and 50% of the amount of CO_2 that could be adsorbed by coating each new grain with a monolayer of CO_2. Each adsorbed CO_2 molecule occupies an area between 22 (monolayer) and 100 (observed) $Å^2$. Assuming Barker and Torkelson's data using crystalline basalts and quartz can be extended to basaltic glasses, 2–7 pmol CO_2 can be adsorbed per mm^2 of freshly created glass surface. In the worst-case scenario, where a CO_2 monolayer is adsorbed on all freshly crushed surfaces, 750 mg of 100 μm diameter spherical grains are required to adsorb a significant fraction (25%) of the 0.5 μmol CO_2 that is typically released from each crush step. Considering that <200 mg of any sample is crushed to less than 100 μm (Table 2), it seems unlikely that CO_2 adsorption can account for the large differences in noble gas/CO_2 ratio observed from sample to sample. However, CO_2 adsorption may be significant for the final crush steps or for gas-poor samples that yielded less CO_2. For example, crush steps that yielded only 0.05 μmol of CO_2 (e.g., sample AMK3339, the final step of AMK3373 and the first step of AMK3377) require only 75 mg of <100 micron powder to adsorb 25% or more of the released gas. In these instances, it is plausible that noble gas:CO_2 measurements systematically overestimate the true ratios.

[41] While some of the variations in noble gas/CO_2 can be attributed to CO_2 adsorption during analysis, there is a smaller range in $^4He/CO_2$ compared to $^{40}Ar^*/CO_2$ and most samples have a range in $^4He/^{40}Ar^*$. These cannot result from CO_2 adsorption; therefore there are real variations in noble gas/CO_2 in the vesicles (Figure 6). The variations are consistent with solubility controlled degassing which would fractionate $^4He/CO_2$ less than $^{40}Ar^*/CO_2$.

5.5.2. The Dataset as a Whole

[42] Although some CO_2 adsorption occurs during analysis, the $^{40}Ar^*/CO_2$ variation in the dataset as a whole is considerably greater than the variation in $^{40}Ar^*/CO_2$ within multiple crushes of a single sample. If CO_2 adsorption was the dominant control on noble gas-CO_2 fractionation, then the variation within a single sample should be similar to that of the dataset as a whole: clearly this is not so. Furthermore, most of the variation within individual samples results from high $^{40}Ar^*/CO_2$ in the final crush steps; if CO_2 adsorption during analysis was the major noble gas-CO_2 fractionation mechanism, excluding the final crush steps should reduce or eliminate the overall $^{40}Ar^*/CO_2$ variation. Again, this is not so (Figure 6). While CO_2 adsorption does affect the analyses – particularly the last crush of each sample – it seems likely some other mechanism must fractionate CO_2 from the noble gases in order to generate the range in $^{40}Ar^*/CO_2$ and $^4He/CO_2$ observed within the dataset as a whole. Solubility-determined fractionation cannot account for these variations as there is a restricted range in $^4He/^{40}Ar^*$ but large range in He/CO_2; while volatile solubilities in melts are dependent on melt composition (and pressure), Ar is always less soluble than either He or CO_2 [*Carroll and Webster*, 1994; *Dixon et al.*, 1995; *Jendrzewski et al*, 1997; *Mattey*, 1991], consequently He and Ar should fractionate more than He and CO_2.

[43] The reason behind these large variations in ^4He or $^{40}Ar^*/CO_2$ is not obvious. Plausible mechanisms include the following: (1) there are large variations in the volatile chemistry of the basalt source regions; (2) the mantle source has relatively constant noble gas/CO_2 but variations in mantle melting conditions (fraction melted or F_{O_2} during melting) result in primary melts with different noble gas/CO_2 ratios; and (3) the mantle and the primary melts have constant noble gas/CO_2 but late stage fractionation of C species from noble gases results in the highly variable noble gas/CO_2 ratios observed.

[44] Variations in the mantle $^4He/CO_2$ (#1) or in the melting regime (#2) should be accompanied by variations in other geochemical tracers (either solid or volatile). A decrease in noble gas/CO_2 of approximately 10-fold is not reflected in $^3He/^4He$, major element composition or Sr isotopic composition, as might be expected of melting in the presence of CO_2 [*Hirschmann*, 2000], or if (for example) recycling introduced C to the mantle source. This suggests a more shallow origin of the noble gas-CO_2 fractionation.

[45] It is possible that solid C can be stabilized in a magma, which would result in high noble gas/CO_2 ratios in the volatile phase, as observed in these samples. For example, solid (at room temperature), reduced C species have been observed in basaltic glasses, although their origin, reduced magmatic C or a posteruption contaminant, remain controversial [e.g., *Mattey*, 1991; *Pineau and Javoy*, 1994]. If C reduction does occur within the magma (as proposed by *Mathez and Delany* [1981] and *Pineau and Javoy* [1994]) or during cooling of the glass, then decoupled noble gas – CO_2 behavior would result, possibly creating the large range in noble gas/CO_2 observed in this sample set. Other mechanisms for fractionating noble gases from CO_2 cannot be ruled out, for example, it is conceivable that this is a kinetic effect where noble gases diffuse rapidly and therefore attain melt – vapor equilibration, while comparatively slow CO_2 diffusion prevents CO_2 equilibration. This is consistent with measurements of CO_2 contents in EPR basalts [*Dixon et al.*, 1988] that show CO_2 is overpressured in the glass relative to the vesicles. The overall trend for high noble gas/CO_2 ratios at low CO_2 concentrations (Figure 7) is broadly consistent with preferential CO_2 removal from the vesicles but does not discriminate between these mechanisms.

6. Conclusions

[46] Complex processes determine the noble gas abundances and isotope ratios measured in basaltic glasses. There are at least four sources of noble gases in these samples, only one of which originated in the mantle. The remaining three noble gas sources are all atmospheric noble gases that have been fractionated relative to each other. These most likely were added to the mantle-derived noble gases after eruption: there is no evidence for significant contamination of the magma itself. The most shallow ridge segment sampled has the highest fraction of atmospheric-derived gases.

[47] The noble gases in the mantle-derived contribution to the noble gas budget have also fractionated from each other. Fractionation during solubility-determined gas loss from the magma resulted in high $^4He/^{40}Ar^*$ in small vesicles (as sampled by later crushes). Although the lowest concentrations of volatiles are found in samples from the shallowest ridges, there is no relation with amount of degassing (as traced by $^4He/^{40}Ar^*$) with either ridge depth or location of eruption on the segment. Degassing is thought to be dominated by deeper, mid-crustal processes.

[48] As a result of the complex contamination processes, it is difficult to constrain the mantle $^{40}Ar/^{36}Ar$ ratio other than the mantle source of Ar in these samples are not distinguishable from that of the ''popping rock'' ($^{40}Ar/^{36}Ar$ = 40,000–80,000; [*Harrison et al.*, 2002]).

[49] Noble gas:CO_2 ratios are highly variable. While the extreme ratios (typically of very low gas releases) may result from analytical artifacts, the range observed in these measurements likely reflect the range actually present in the vesicles. The large variations in noble gas: CO_2 cannot result from solubility-determined gas loss from the magma, but may result from CO_2 disproportionation and condensation of reduced C species within the vesicles during cooling.

Acknowledgments

[50] This manuscript was considerably improved by comments from Manuel Moreira, Masahiko Honda and an anonymous reviewer. Don Porcelli first suggested using ''Turnery Diagram'' for the three-axis plots. PB and DH were funded by the Natural Environment Research Council of Great Britain.

References

Allègre, C. J., T. Staudacher, and P. Sarda, Rare gas systematics: Formation of the atmosphere, evolution and structure of the Earth's mantle, *Earth Planet. Sci. Lett.*, *81*, 127–150, 1986.

Ballentine, C. J., and D. N. Barfod, The origin of air-like noble gases in MORB and OIB, *Earth Planet. Sci. Lett.*, *180*, 39–48, 2000.

Barker, C., and B. E. Torkelson, Gas adsorption of crushed quartz and basalt, *Geochim. Cosmochim. Acta*, *55*, 212–218, 1975.

Burnard, P. G., The bubble-by-bubble volatile evolution of two mid-ocean ridge basalts, *Earth Planet. Sci. Lett.*, *174*, 199–211, 1999a.

Burnard, P. G., Origin of Argon-Lead isotopic correlations in basalts, *Science*, *286*, 871, 1999b.

Burnard, P., Correction for volatile fractionation in ascending magmas: Noble gas abundances in primary mantle melts, *Geochim. Cosmochim. Acta*, *65*, 2605–2614, 2001.

Burnard, P. G., D. W. Graham, and K. A. Farley, Noble gas constraints on magmatic gas loss along the Southeast Indian Ridge and the Amsterdam - St. Paul Plateau, *Earth Planet. Sci. Lett.*, *203*, 131–148, 2002.

Carroll, M. R., and E. M. Stolper, Noble gas solubilities in silicate melts and glasses: New experimental results for argon and the relationship between solubility and ionic porosity, *Geochim. Cosmochim. Acta*, *57*, 5039–5052, 1993.

Carroll, M. R., and J. D. Webster, Solubilities of sulfur, noble gases, nitrogen, chlorine and fluorine in magmas, in *Volatiles in Magmas*, edited by M. R. Carroll and J. R. Holloway, pp. 231–271, Mineral. Soc. of Am., Washington, D.C., 1994.

Dixon, J. E., and E. Stolper, An experimental study of water and carbon dioxide solubilities in mid - ocean ridge basaltic liquids, Part II, Applications to degassing, *Contrib. Mineral. Petrol.*, *36*, 1633–1646, 1995.

Dixon, J. E., E. Stolper, and J. R. Delaney, Infrared spectroscopic measurements of CO_2 and H_2O in Juan de Fuca Ridge basaltic glasses, *Earth Planet. Sci. Lett.*, *90*, 87–104, 1988.

Farley, K. A., and E. Neroda, Noble gases in the Earth's mantle, *Ann. Rev. Earth Planet. Sci.*, *26*, 189–218, 1998.

Farley, K. A., and R. J. Poreda, Mantle neon and atmospheric contamination, *Earth Planet. Sci. Lett.*, *114*, 325–339, 1993.

Fisher, D. E., Helium, argon, and xenon in crushed and melted MORB, *Geochim. Cosmochim. Acta*, *61*, 3003–3012, 1997.

Harrison, D. W., P. G. Burnard, and G. Turner, Noble gas behaviour and composition in the mantle: Constraints from the Iceland Plume, *Earth Planet. Sci. Lett.*, *171*, 199–207, 1999.

Harrison, D., P. Burnard, M. Trieloff, and G. Turner, Resolving atmospheric contaminants in mantle noble gas analyses, *Geochem. Geophys. Geosyst.*, doi:10.1029/2002GC000325, in press, 2002.

Hirschmann, M. M., Mantle solidus: Experimental constraints and the effects of peridotite composition, *Geochemistry, Geophysics, Geosystems*, *1*, Paper number 2000GC000070, 2000.

Honda, M., and D. B. Patterson, Systematic elemental fractionation of mantle-derived helium, neon, and argon in mid-oceanic ridge glasses, *Geochim. Cosmochim. Acta*, *63*, 2863–2874, 1999.

Honda, M., I. McDougall, D. B. Patterson, A. Doulgeris, and D. A. Clague, Noble gases in submarine pillow basalt glasses from Loihi and Kilauea, Hawaii; A solar component in the Earth, *Geochim. Cosmochim. Acta*, *57*, 859–874, 1993.

Jambon, A., H. W. Weber, and F. Begeman, Helium and argon from an Atlantic MORB glass: concentration, distribution and isotopic composition, *Earth Planet. Sci. Lett.*, *73*, 255–267, 1985.

Jambon, A., H. Weber, and O. Braun, Solubility of He, Ne, Ar, Kr and Xe in a basalt melt in the range 1250–1600°C, *Geochemical implications, Geochim. Cosmochim. Acta*, *50*, 401–408, 1986.

Javoy, M., and F. Pineau, The volatiles record of a "popping" rock from the Mid-Atlantic Ridge at 14 N: Chemical and isotopic composition of gas trapped in the vesicles, *Earth Planet. Sci. Lett.*, *107*, 598–611, 1991.

Jendrzejewski, N., T. W. Trull, F. Pineau, and M. Javoy, Carbon solubility in mid-ocean ridge basaltic melt at low pressures (250–1950 bar), *Chem. Geol.*, *138*, 81–92, 1997.

Kurz, M. D., and W. J. Jenkins, The distribution of helium in oceanic basalt glasses, *Earth Planet. Sci. Lett.*, *53*, 41–54, 1981.

Lux, G., The behaviour of noble gases in silicate liquids: solution, diffusion, bubbles and surface effects, with applications to natural samples, *Geochim. Cosmochim. Acta*, *51*, 1549–1560, 1987.

Marty, B., and L. Zimmerman, Volatiles (He, C, N, Ar) in mid-ocean ridge basalts: Assessment of shallow level fractionation and characterization of source composition, *Geochim. Cosmochim. Acta*, *63*, 3619–3633, 1999.

Mathez, E. A., and J. R. Delany, The nature and distribution of carbon in submarine basalts and peridotite nodules, *Earth Planet. Sci. Lett.*, *56*, 217–232, 1981.

Matsubara, K., and J.-I. Matsuda, Anomalous Ne enrichments in tektites, *Meteoritics*, *26*, 217–220, 1991.

Matsuda, J.-I., and B. Marty, The $^{40}Ar/^{36}Ar$ ratio of the undepleted mantle; a reevaluation, *Geophys. Res. Lett.*, *22*, 1937–1940, 1995.

Mattey, D. P., Carbon dioxide solubility and carbon isotope fractionation in basaltic melt, *Geochim. Cosmochim. Acta*, *55*, 3467–3473, 1991.

Moreira, M., and C. J. Allègre, Rare gas systematics on Mid Atlantic Ridge (37–40°N), *Earth and Planetary Science Letters*, *198*, 401–416, 2002.

Moreira, M., J. Kunz, and C. Allègre, Rare gas systematics in popping rock: Isotopic and elemental compositions in the upper mantle, *Science*, *279*, 1178–1181, 1998.

Pan, V., J. R. Holloway, and R. L. Hervig, The pressure and temperature dependence of carbon dioxide solubility in tholeiitic basalt melts, *Geochim. Cosmochim. Acta*, *55*, 1587–1595, 1991.

Patterson, D. B., M. Honda, and I. McDougall, Atmospheric contamination: a possible source for heavy noble gases in basalts from Loihi Seamount, Hawaii, *Geophys. Res. Lett.*, *17*, 705–708, 1990.

Pineau, F., and M. Javoy, Strong degassing at ridge crests: The behaviour of dissolved carbon and water in basalt glasses at 14°N, Mid - Atlantic Ridge, *Earth Planet. Sci. Lett.*, *123*, 179–198, 1994.

Sarda, P., and M. Moreira, Vesiculation and vesicle loss in mid-ocean ridge basalt glasses: He, Ne, Ar elemental fractionation and pressure influence, *Geochim. Cosmochim. Acta.*, *66*, 1449–1458, 2002.

Sarda, P., T. Staudacher, and C. Allègre, Neon isotopes in submarine basalts, *Earth Planet. Sci. Lett.*, *91*, 73–88, 1988.

Sarda, P., M. Moreira, and T. Staudacher, Argon-lead isotopic correlation in Mid-Atlantic Ridge basalts, *Science*, *283*, 666–668, 1999.

Sarda, P., M. Moreira, T. Staudacher, J.-G. Schilling, and C. J. Allègre, Rare gas systematics on the southernmost Mid-Atlantic Ridge: Constraints on the lower mantle and the Dupal source, *J. Geophys. Res.*, *105*, 5973–5996, 2000.

Trieloff, M., J. Kunz, D. A. Clague, D. Harrison, and C. J. Allègre, The nature of pristine noble gases mantle plumes, *Science*, *288*, 1036–1038, 2000.

Trieloff, M., J. Kunz, and C. J. Allègre, Noble gas systematics of the Réunion mantle plume source and the origin of primordial noble gases in Earth 's mantle, *Earth Planet. Sci. Lett.*, *200*, 297–313, 2002.

Valbracht, P. J., T. Staudacher, A. Malahoff, and C. J. Allègre, Noble gas systematics of deep riftzone glasses from Loihi Seamount, Hawaii, *Earth Planet. Sci. Lett.*, *150*, 399–411, 1997.